

# Synthesis and Characterization of Mo<sub>2</sub>C/MoO<sub>3</sub> Nanohybrid as Electrocatalyst for Hydrogen Evolution Reaction

Maria Sarno, Claudia Cirillo\*, Eleonora Ponticorvo, Paolo Ciambelli

Department of Industrial Engineering and Centre NANO\_MATES, University of Salerno, Via Giovanni Paolo II, 132 - 84084 Fisciano (SA), Italy  
ccirillo@unisa.it

The two-step preparation of core-shell Mo<sub>2</sub>C/MoO<sub>3</sub> nanoplatelets (composed of an MoO<sub>3</sub> core covered by 3 nm Mo<sub>2</sub>C outer layer) is reported. The process consists of the thermolysis of a solid precursor, ammonium molybdate ((NH<sub>4</sub>)<sub>6</sub>Mo<sub>7</sub>O<sub>24</sub>·4H<sub>2</sub>O), in a reactor fed by nitrogen (200 cm<sup>3</sup>(STP)/min), heated from room temperature to 700 °C, followed by a controlled Chemical Vapor Deposition (CVD) of CH<sub>4</sub>, 10 v/v % in nitrogen, for 10 minutes, monitored on - line by continuous gas analyzers.

A Tafel slope of 48 mV/decade was measured for the Mo<sub>2</sub>C/MoO<sub>3</sub> nanohybrid suggesting the Volmer-Heyrovsky mechanism for the nanohybrid-catalyzed HER. MoO<sub>3</sub> deserves as a highly nanostructured conductive core, while the thin Mo<sub>2</sub>C coating serves as both a HER catalyst and a protective layer.

## 1. Introduction

Hydrogen is being vigorously pursued as an ideal energy carrier and its production by water splitting is attracting growing attention. The electrolysis efficiency is enhanced when Pt is used as the catalyst in acidic media. In particular, the main effective catalysts are Pt-group metals but it remains challenging to look for alternative catalysts that are more abundant and at lower cost. Group VI transition metal carbides exhibit catalytic properties analogous to platinum group metals because of their unique d-band electronic structures. Tungsten carbide has been explored for the Hydrogen Evolution Reaction (HER) providing interesting results, but with a high overpotential if compared with Pt-group metals (Esposito and Chen, 2011). On the other hand, molybdenum carbide was been demonstrated able to reduce the overpotential (Chen et al., 2013).

Many approaches including Chemical Vapour Deposition (CVD) (Hanif et al., 2002) and pyrolysis of metal complexes (Wolden et al., 2011) have been developed for the preparation of metal carbides. Among them the more explored is CVD using hydrocarbons (Giubileo et al., 2012) or carbonaceous gases (e.g. CO) and Mo gaseous precursors (MoF<sub>6</sub>, Mo(CO)<sub>6</sub>, MoCl<sub>5</sub>). However, the gas-phase syntheses generally required elaborate equipment, involve the use of expensive and toxic reagents, and the product is usually contaminated by chars from the pyrolysis of carbonaceous gases.

Here we report the preparation of core-shell Mo<sub>2</sub>C/MoO<sub>3</sub> nanoplatelets by a solid precursor thermolysis under nitrogen, followed by a controlled CVD of CH<sub>4</sub>.

The characterization was obtained by the combined use of different physico-chemical techniques, and the Mo<sub>2</sub>C/MoO<sub>3</sub> nanohybrid was characterized for HER.

## 2. Experimental

Core-shell Mo<sub>2</sub>C/MoO<sub>3</sub> nanoplatelets were prepared by a solid precursor (ammonium molybdate (NH<sub>4</sub>)<sub>6</sub>Mo<sub>7</sub>O<sub>24</sub>·4H<sub>2</sub>O) thermolysis under a nitrogen (200 cm<sup>3</sup>(STP)/min) flow, in a continuous flow reactor (Di Bartolomeo et al., 2009), from room temperature to 700°C, followed by a controlled CVD (Ciambelli et al., 2004) of CH<sub>4</sub> (Sarno et al., 2012b) 10 v/v % in nitrogen for 10 min.

Methane CVD was carried out by feeding, at 700 °C (controlled by a K thermocouple), a methane–nitrogen gas mixture on the reaction bed. The reactor was heated by an electrical oven which temperature was controlled by a temperature programmer–controller (Eurotherm 2408). Cylinder gases (99.998 pure methane and 99.9990 pure nitrogen) were mixed to obtain the methane/nitrogen stream that was fed to the reactor. A constant flow rate of each gas was provided by a mass flow controller. The experimental plant for the synthesis was equipped with on-line ABB analyzers (Sarno et al., 2012a) that permit to monitor the concentrations in the effluent stream (Sarno et al., 2013b) of the following chemicals during the reaction: methane (CH<sub>4</sub>) the source of carbon, ethylene (C<sub>2</sub>H<sub>4</sub>), acetylene (C<sub>2</sub>H<sub>2</sub>) and H<sub>2</sub>.

The characterization was obtained by the combined use of different techniques. Transmission electron microscopy (TEM) images were obtained using a FEI Tecnai electron microscope operated at 200 kV with a LaB<sub>6</sub> filament as the source of electrons, equipped with an EDX probe. Scanning electron microscopy (SEM) images were obtained with a LEO 1525 microscope. Raman spectra were obtained at room temperature with a micro-Raman spectrometer Renishaw inVia with a 514 nm excitation wavelength (laser power 30 mW) in the range 100–1100 cm<sup>-1</sup>. Optical images were collected with a Leica DMLM optical microscope connected on-line with the Raman instrument. The laser spot diameter was about 10 μm. XRD measurements were performed with a Bruker D8 X-ray diffractometer using CuKα radiation. Thermogravimetric analysis (TG-DTG) at a 10 K/min heating rate in flowing air was performed with a SDTQ 600 Analyzer (TA Instruments) coupled with a mass spectrometer. For the electrochemical measurements 4 mg of catalyst were dispersed in 80 μl of 5 wt. % nafion solution to form a homogeneous ink. Then the catalyst ink was loaded onto a glassy carbon electrode of 3 mm in diameter. Linear sweep voltammetry (using the potentiostat from Amel Instruments) with scan rate of 2 mVs<sup>-1</sup> was conducted in 0.5 M H<sub>2</sub>SO<sub>4</sub>, using saturated calomel electrode as the reference electrode, a graphite electrode as the counter electrode and a loadable glassy carbon electrode as the working electrode.

### 3. Results and discussion

Figure 1a shows the diffraction pattern recorded for the Mo<sub>2</sub>C/MoO<sub>3</sub> sample. The typical peaks of orthorhombic α-MoO<sub>3</sub> (Stoyanova et al., 2009) and β-Mo<sub>2</sub>C phases were observed (Chen et al., 2013). The Raman spectrum of the sample excited by 514 nm line in air ambient environment is shown in Figure 1b. It is worth to notice that the spectrum has been obtained at 0.1 % of laser power and after 10 s exposition time, because under more stricter conditions the typical Raman spectrum of MoO<sub>3</sub> appears generated by the laser, which photon energy closely resonant with the electronic absorption and the band gap energies, determines heating/photochemistry via direct absorption (Cervantes-Gaxiola et al., 2013). The typical bands of MoO<sub>3</sub> and Mo<sub>2</sub>C can be seen in Figure 1b. The laser Raman spectrum of Mo<sub>2</sub>C (Figure 3a) is very similar to that of MoO<sub>3</sub>. In particular, the typical vibration frequencies of MoO<sub>3</sub> at 994 cm<sup>-1</sup> and 819 cm<sup>-1</sup> (Frauwallner et al., 2011) and of Mo<sub>2</sub>C at 1006 cm<sup>-1</sup> and 828 cm<sup>-1</sup> (Xiao et al., 2001), can be seen in our spectrum.

Figure 2 shows the representative SEM images for the Mo<sub>2</sub>C/MoO<sub>3</sub> product, at increasing magnifications. The sample has a platelet elongated shape structure and thickness of few nanometers, as shown in Figure 2b.

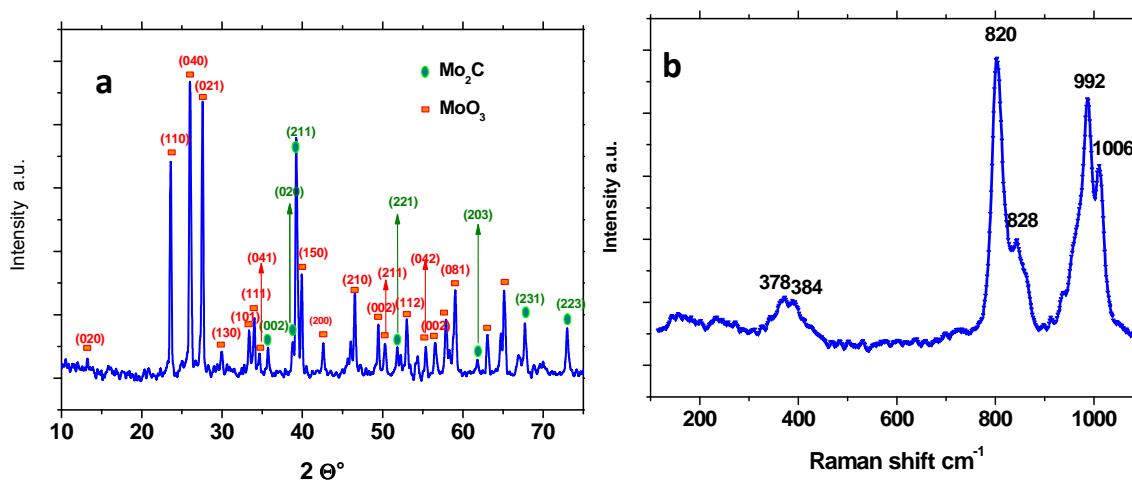


Figure 1: XRD diffraction patterns (a) and Raman spectrum (b) of Mo<sub>2</sub>C/MoO<sub>3</sub>.

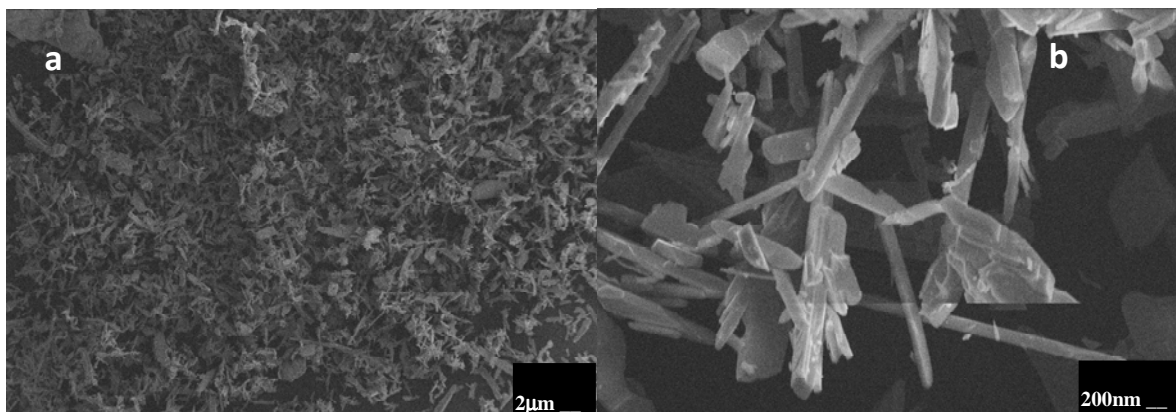


Figure 2: SEM images of  $\text{Mo}_2\text{C}/\text{MoO}_3$  hybrid at different magnifications

TEM investigations carried out, to provide further insights into the morphology, on the resulting  $\text{Mo}_2\text{C}/\text{MoO}_3$  nanostructures, are reported in Figures 3a and 3b at increasing magnifications. Figure 3a shows a typical TEM image at low magnification for the sample confirming the morphology already observed by SEM (Figure 2b). Figure 3b shows that the nanoplatelets are indeed composed of an  $\text{MoO}_3$  core and of a 3 nm  $\text{Mo}_2\text{C}$  outer layer, as confirmed by the selected area diffraction pattern in the Figure 3b insert showing the typical crystallographic in plane square structure ascribable to  $\text{Mo}_2\text{C}$ .

During the precursor thermolysis from room temperature to 700 °C, a weight loss appears below 300 °C, arising from the decomposition of ammonium molybdate (Sarno et al., 2014b), with the formation of  $\text{MoO}_3$  (Delporte et al., 1995). At 700 °C, before sublimation that occurs at around 800 °C (Sarno et al., 2014b), the incorporation of C, coming from the decomposition of  $\text{CH}_4$ , begins by filling  $\text{MoO}_3$  anionic vacancies (Frauwallner et al., 2011). In particular, the evolutions of the concentration profiles of  $\text{CH}_4$  the source of carbon,  $\text{C}_2\text{H}_2$ ,  $\text{C}_2\text{H}_4$  and  $\text{H}_2$  during the isotherm at 700 °C, are shown in Figure 4a.

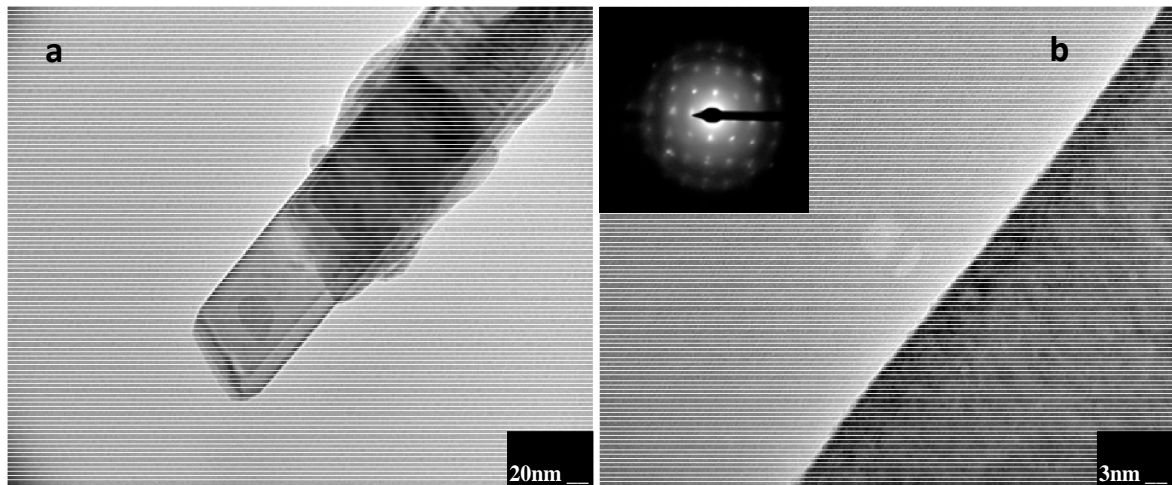


Figure 3: TEM images of  $\text{Mo}_2\text{C}/\text{MoO}_3$  at different magnifications (a, b). SAED pattern of  $\text{Mo}_2\text{C}$  obtained on the edge of the platelets (b insert).

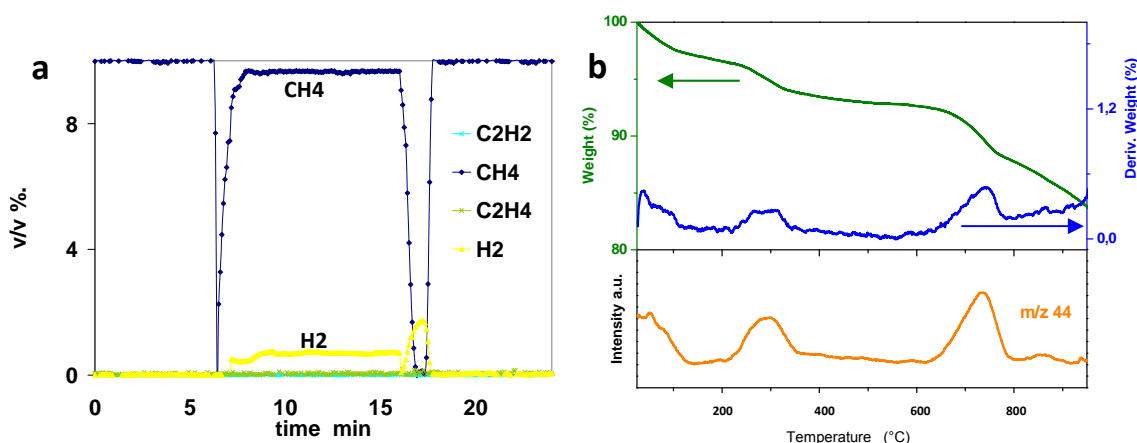


Figure 4: Profiles of  $\text{CH}_4$ ,  $\text{C}_2\text{H}_4$ ,  $\text{C}_2\text{H}_2$  and  $\text{H}_2$  concentrations during the  $\text{Mo}_2\text{C}/\text{MoO}_3$  synthesis at  $700^\circ\text{C}$  (a). TG-DTG profiles of the  $\text{Mo}_2\text{C}/\text{MoO}_3$  as prepared and the corresponding total ion current of  $\text{CO}_2$  (b)

Observing Figure 4a, three temporal phases (Sarno et al., 2014a) can be distinguished:

- Pre-reaction phase (I): the reaction gas is fed to the analyzers. All of the concentration values are close to zero, except for the initial methane concentration, which is 10 v/v %.
- Reaction phase (II): the gases are fed to the reactor, reaching the analyzers after passing through the catalyst bed. After the time necessary to pass the reactor and accounting for the delay time of the analyzers, the steady state methane concentration stabilizes at 9.58 v/v %, while the hydrogen concentration in the effluent stream shows the opposite trend and stabilizes at 0.69 v/v %. No significant  $\text{C}_2\text{H}_4$  and  $\text{C}_2\text{H}_2$  concentrations are detected during the entire running time at the chosen temperature ( $700^\circ\text{C}$ ).
- Post-reaction phase (III): the reaction has ended, and the gases are sent directly back to the analyzers (bypassing the reactor). The concentrations of the four gases are the same as those in the pre-reaction phase. The amount of carbon coming from the decomposition of methane is calculated by the conversion of methane (data from Figure 4a) (Sarno et al., 2013a), considering the volumes and densities of  $\text{MoO}_3$  and  $\text{Mo}_2\text{C}$ . This result is compatible with the formation of a  $\text{Mo}_2\text{C}$  layer of about 3 nm around the  $\text{MoO}_3$  platelet.

In Figure 4b the thermogravimetric (TG-DTG) profiles, of the synthesized  $\text{Mo}_2\text{C}/\text{MoO}_3$  nanohybrid, are reported as function of temperature. As clearly indicated by the corresponding TIC of  $\text{CO}_2$  ( $m/z = 44$ ), two weight losses due to carbon are visible: (i) in the range  $200\text{--}400^\circ\text{C}$ , probably due to few percents of carbon impurities, coming from the methane homogeneous decomposition; and in the range  $580\text{--}800^\circ\text{C}$  due to the  $\text{Mo}_2\text{C}$  oxidation to form molybdenum trioxide and carbon dioxide (Chen et al., 2013), this is partially superimposed with the sublimation of  $\text{MoO}_3$  which begins at around  $750^\circ\text{C}$ , as previously reported (Chen et al., 2013).

The electrocatalytic HER activities of  $\text{Mo}_2\text{C}/\text{MoO}_3$  were investigated. The hybrid material was deposited on a glassy carbon electrode in  $0.5\text{ M H}_2\text{SO}_4$  solution using a typical three-electrode setup. As a reference point, a commercial Pt catalyst with known high HER catalytic performances was evaluated (Sarno et al., 2014c). The results are shown in Figure 5. Polarization curve (i-V plot) recorded for  $\text{Mo}_2\text{C}/\text{MoO}_3$  (Figure 5a) showed an overpotential of  $\sim 0.13\text{ V}$  for HER, beyond which the cathodic current rose rapidly under more negative potentials. Linear portions of the Tafel plots (Figure 5b) were fit to the Tafel equation ( $\eta = b \log j + a$ , where  $\eta$  is the overpotential,  $j$  is the current density,  $b$  is the Tafel slope), yielding Tafel slopes of  $\sim 30$  and  $\sim 48\text{ mV/decade}$  (iR-corrected) for Pt, and  $\text{Mo}_2\text{C}/\text{MoO}_3$  nanohybrid, respectively. The observed Tafel slope for  $\text{Mo}_2\text{C}/\text{MoO}_3$  suggests that electrochemical desorption is the rate limiting step (Li et al., 2011), the high performance is probably due to the electrocatalytic activity of  $\text{Mo}_2\text{C}$  and an electronic coupling with the highly conductive  $\text{MoO}_3$  (Li et al., 2011).

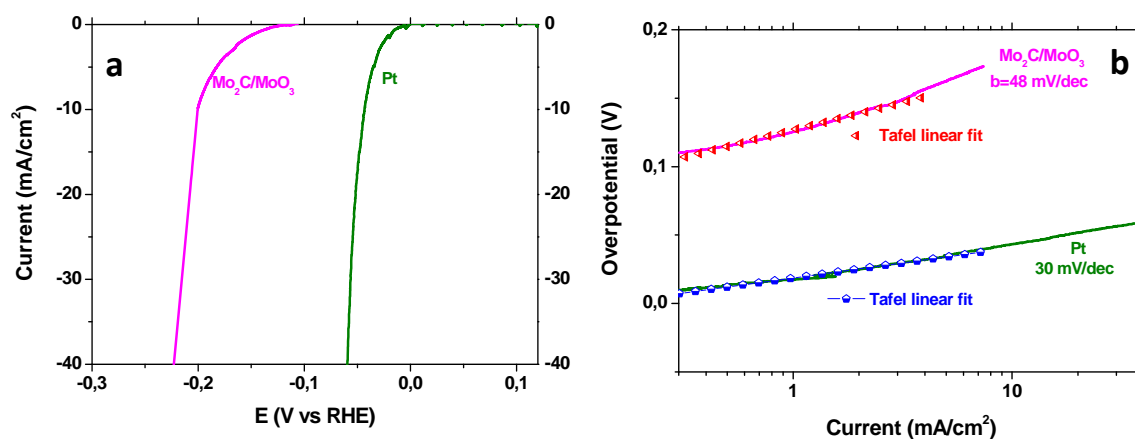


Figure 5: Polarization curves obtained (a), and corresponding Tafel plots (b).

#### 4. Conclusions

Core-shell  $\text{Mo}_2\text{C}/\text{MoO}_3$  nanoplatelets have been prepared by a solid precursor thermolysis, avoiding the more complicated and dangerous supply of a molybdenum precursor from the gas phase, followed by a controlled CVD of  $\text{CH}_4$ , monitored on-line by ABB analyzers.

The characterization confirms the nature of the material, that shows excellent HER activity, with a Tafel slope of 48 mV/dec compatible with electrochemical desorption as rate limiting step. The  $\text{Mo}_2\text{C}/\text{MoO}_3$  nano-hybrid is able to efficiently drive the HER due to  $\text{MoO}_3$  working as a highly nanostructured conductive core, while the thin  $\text{Mo}_2\text{C}$  coating serves as both a HER catalyst and a protective layer.

#### References

- Cervantes-Gaxiola M. E., Arroyo-Albiter M., Pérez-Larios A., Balbuena P. B., Espino-Valencia J., 2013, Experimental and theoretical study of NiMoW, NiMo, and NiW sulfide catalysts supported on an Al-Ti-Mg mixed oxide during the hydrosulfurization of dibenzothiophene, *Fuel*, 113, 733–743.
- Chen W. F., Wang C.H., Sasaki K., Marinkovic N., Xu W., Muckerman J. T., Zhu Y., Adzic R.R., 2013, Highly Active, Durable, and Nanostructured Molybdenum Carbide Electrocatalysts for Hydrogen Production, *Energy Environ. Sci.* 6, 943-951.
- Chen Z., Cummins D., Reinecke B.N., Clark E., Sunkara M.K., Jaramillo T.F., 2011, Core-shell  $\text{MoO}_3$ - $\text{MoS}_2$  Nanowires for Hydrogen Evolution: A Functional Design for Electrocatalytic Materials, *Nano Lett.* 11, 4168-4175.
- Ciambelli P., Sannino D., Sarno M., Nagy, J.B., 2004, Characterization of nanocarbons produced by CVD of ethylene in alumina or alumino-silicate matrices, *Adv. Eng. Mater.* 6, 804-811.
- Delporte P., Meunier F., Cuong P.H., Venegues P., Ledoux M. J., Guille J., 1995, Physical characterization of molybdenum oxycarbide catalyst: TEM, XRD and XPS, *Catal. Today* 23, 251-267.
- Di Bartolomeo A., Sarno M., Giubileo F., Altavilla C., Iemmo L., Piano S., Bobba F., Longobardi M., Scarfato A., Sannino D., Cucolo A.M., Ciambelli P., 2009, Multiwalled carbon nanotube films as small-sized temperature sensors, *J. Appl. Phys.* 105, 064518.
- Esposito D.V., Chen J.G., 2011, Monolayer Platinum Supported on Tungsten Carbides as Low-Cost Electrocatalysts: Opportunities and Limitations, *Energy Environ. Sci.* 4, 3900-3912.
- Frauwaller M.L., López-Linares F., Lara-Romero J., Scott C.E., Ali V., Hernández E., Pereira-Almao P., 2011, Toluene hydrogenation at low temperature using a molybdenum carbide catalyst, *Appl. Catal. A: General*, 394, 62-70.
- Giubileo F., Di Bartolomeo A., Sarno M., Altavilla C., Santandrea S., Ciambelli P., Cucolo A.M., 2012, Field emission properties of as-grown multiwalled carbon nanotube films, *Carbon*, 50, 163-169.
- Hanif A., Xiao T., York A.P.E., Sloan J., Green M.L.H., 2002, Study on the Structure and Formation Mechanism of Molybdenum Carbides, *Chem. Mater.* 14, 1009-1015.
- Li Y., Wang H., Xie L., Liang Y., Hong G., Dai H., 2011,  $\text{MoS}_2$  Nanoparticles Grown on Graphene: An Advanced Catalyst for the Hydrogen Evolution Reaction, *J. Am. Chem. Soc.* 133, 7296-7299.

- Sarno M., Cirillo C., Piscitelli R., Ciambelli P., 2013a, A study of the key parameters, including the crucial role of H<sub>2</sub> for uniform graphene growth on Ni foil, *J. Mol. Catal. A: Chem.* 366, 303-314.
- Sarno M., Sannino D., Leone C., Ciambelli P., 2012a, Evaluating the effects of operating conditions on the quantity, quality and catalyzed growth mechanisms of CNTs, *J. Mol. Catal. A: Chem.* 357, 26-38.
- Sarno M., Sannino D., Leone C., Ciambelli P., 2012b, CNTs tuning and vertical alignment in anodic aluminium oxide membrane, *J. Nat. Gas. Chem.* 21, 639-646.
- Sarno M., Tamburrano A., Arurault L., Fontorbes S., Pantani R., Datas L., Ciambelli P., Sarto M.S., 2013b, Electrical conductivity of carbon nanotubes grown inside a mesoporous anodic aluminium oxide membrane, *Carbon*, 55, 10-22.
- Sarno M., Cirillo C., Ciambelli P., 2014a, Selective graphene covering of monodispersed magnetic nanoparticles, *Chem. Eng. J.* 246, 27-38.
- Sarno M., Garamella A., Cirillo C., Ciambelli P., 2014b, MoO<sub>2</sub> Synthesis for LIBs, *Chemical Engineering Transaction*, 41, 307-312. DOI: 10.3303/CET1441052
- Sarno M., Garamella A., Cirillo C., Ciambelli P., 2014c, MoS<sub>2</sub>/MoO<sub>2</sub>/Graphene Electrocatalyst for HER, *Chemical Engineering Transaction*, 41, 385-390. DOI: 10.3303/CET1441065
- Stoyanova A., Iordanova R., Mancheva M., Dimitriev Y., 2009, Synthesis and structural characterization of MoO<sub>3</sub> phases obtained from molybdic acid by addition of HNO<sub>3</sub> and H<sub>2</sub>O<sub>2</sub>, *J. Optoelectron. Adv. M.* 11, 1127-1131.
- Wolden C.A., Pickerell A., Gawai T., Parks S., Hensley J., Way J.D., 2011, Synthesis of β-Mo(2)C thin films, *ACS Appl. Mater. Interfaces*, 3, 517-521.
- Xiao T.C., York A.P.E., Al-Megren H., Williams C.V., Wang H.T., Green M.L.H., 2001, Preparation and Characterisation of Bimetallic Cobalt and Molybdenum Carbides, *J. Catal.* 202, 100-109.